RESEARCH ARTICLE SUMMARY

MARTIAN GEOLOGY

Deposition, exhumation, and paleoclimate of an ancient lake deposit, Gale crater, Mars

J. P. Grotzinger,* S. Gupta, M. C. Malin, D. M. Rubin, J. Schieber, K. Siebach, D. Y. Sumner, K. M. Stack, A. R. Vasavada, R. E. Arvidson, F. Calef III, L. Edgar, W. F. Fischer, J. A. Grant, J. Griffes, L. C. Kah, M. P. Lamb, K. W. Lewis, N. Mangold, M. E. Minitti, M. Palucis, M. Rice, R. M. E. Williams, R. A. Yingst, D. Blake, D. Blaney, P. Conrad, J. Crisp, W. E. Dietrich, G. Dromart, K. S. Edgett, R. C. Ewing, R. Gellert, J. A. Hurowitz, G. Kocurek, P. Mahaffy, M. J. McBride, S. M. McLennan, M. Mischna, D. Ming, R. Milliken, H. Newsom, D. Oehler, T. J. Parker, D. Vaniman, R. C. Wiens, S. A. Wilson

INTRODUCTION: Remote observational data suggest that large bodies of standing water existed on the surface of Mars in its early history. This would have required a much wetter climate than that of the present, implying greater availability of water on a global basis and enhanced potential for global habitability. However, based on assumptions of a vast water inventory and models of atmospheric erosion, theoretical studies suggest a climate that was wetter but not by enough to sustain large lakes, even in depressions such as impact craters.

RATIONALE: The Mars Science Laboratory mission's rover, Curiosity, provides the capability to test hypotheses about Mars's past climate. The focus of the mission is the exploration of a ~5-km-high mountain, Aeolis Mons (informally known as Mount Sharp), located near the center of the ~140-km-wide Gale impact crater. Mount Sharp is underlain by hundreds of meters of sedimentary rock strata deposited ~3.6 billion to 3.2 billion years ago. These sediments accumulated in aqueous environments, recording the history of Mars's ancient climate. Because of Curiosity's ability to study these strata where they are exposed near the base of Mount Sharp, we can directly test the hypothesis that large impact craters were capable of accumulating and storing water as lakes for substantial periods of time.

RESULTS: Over the course of 2 years, Curiosity studied dozens of outcrops distributed along a ~9-km transect that also rose ~75 m in elevation. Image data were used to measure the geometry and grain sizes of strata and to survey the textures associated with sediment deposition and diagenesis. Erosion of Gale's northern crater wall and rim generated gravel and sand that were transported southward in shallow streams. Over time, these stream deposits advanced toward the crater interior, transitioning downstream into finer-grained (sand-sized), southward-advancing delta deposits. These deltas marked the boundary of an ancient lake where the finest (mud-sized) sediments accumulated, infilling both the crater and its internal lake basin. After infilling of the crater, the sedimentary deposits in Gale crater were exhumed, probably by wind-driven erosion, creating Mount Sharp. The ancient stream and lake deposits are erosional remnants of superimposed depositional sequences that once extended at least 75 m, and perhaps several hundreds of meters, above the current elevation of the crater floor. Although the modern landscape dips northward away from Mount Sharp, the ancient sedimentary deposits were laid down along a profile that projected southward beneath Mount Sharp and indicate that a basin once existed where today there is a mountain.

ON OUR WEB SITE

Read the full article at http://dx.doi.org/10.1126/science.aac7575

CONCLUSION: Our observations suggest that individual lakes were stable on the ancient surface of Mars for 100 to 10,000 years, a minimum duration when each lake was stable both thermally (as liquid water) and in terms of mass balance (with inputs effectively matching evaporation and loss of water to colder regions). We estimate that the stratigraphy traversed thus far by Curiosity would have required 10,000 to 10,000,000 years to accumulate, and even longer if overlying strata are included. Though individual lakes may have come and gone, they were probably linked in time through a common groundwater table. Over the long term, this water table must have risen at least tens of meters to enable accumulation of the delta and lake deposits observed by Curiosity in Gale crater. ■

Inclined strata in the foreground dip southward toward Mount Sharp and represent ancient delta deposits. These deposits transition into strata in the midfield that were deposited in ancient lakes. The buttes and mesas in the background contain younger deposits that overlie and postdate the lake deposits beneath Mount Sharp. The outcrop in the foreground is about 6 m wide, and the buttes and mesas in the background are hundreds of meters wide and tens of meters high. The image has been white-balanced. [Credit: NASA/Caltech/JPL/MSSS]

The list of author affiliations is available in the full article online.
*Corresponding author. E-mail: grotz@gps.caltech.edu
Cite this article as J. P. Grotzinger *et al.*, *Science* **350**, aac7575 (2015).
DOI: 10.1126/science.aac7575

RESEARCH ARTICLE

MARTIAN GEOLOGY

Deposition, exhumation, and paleoclimate of an ancient lake deposit, Gale crater, Mars

J. P. Grotzinger,[1]* S. Gupta,[2] M. C. Malin,[3] D. M. Rubin,[4] J. Schieber,[5] K. Siebach,[1] D. Y. Sumner,[6] K. M. Stack,[7] A. R. Vasavada,[7] R. E. Arvidson,[8] F. Calef III,[7] L. Edgar,[9] W. F. Fischer,[1] J. A. Grant,[10] J. Griffes,[1] L. C. Kah,[11] M. P. Lamb,[1] K. W. Lewis,[12] N. Mangold,[13] M. E. Minitti,[14] M. Palucis,[1] M. Rice,[15] R. M. E. Williams,[14] R. A. Yingst,[14] D. Blake,[16] D. Blaney,[7] P. Conrad,[17] J. Crisp,[7] W. E. Dietrich,[18] G. Dromart,[19] K. S. Edgett,[3] R. C. Ewing,[20] R. Gellert,[21] J. A. Hurowitz,[22] G. Kocurek,[23] P. Mahaffy,[17] M. J. McBride,[3] S. M. McLennan,[22] M. Mischna,[7] D. Ming,[24] R. Milliken,[25] H. Newsom,[26] D. Oehler,[27] T. J. Parker,[7] D. Vaniman,[14] R. C. Wiens,[28] S. A. Wilson[10]

The landforms of northern Gale crater on Mars expose thick sequences of sedimentary rocks. Based on images obtained by the Curiosity rover, we interpret these outcrops as evidence for past fluvial, deltaic, and lacustrine environments. Degradation of the crater wall and rim probably supplied these sediments, which advanced inward from the wall, infilling both the crater and an internal lake basin to a thickness of at least 75 meters. This intracrater lake system probably existed intermittently for thousands to millions of years, implying a relatively wet climate that supplied moisture to the crater rim and transported sediment via streams into the lake basin. The deposits in Gale crater were then exhumed, probably by wind-driven erosion, creating Aeolis Mons (Mount Sharp).

Substantial bodies of standing water may have existed on the surface of Mars in its early history. Large craters (*1*), the Valles Marineris canyon network (*2*), and even the hemispheric-scale northern plains (*3*) are depressions where water may have pooled. To support such widespread distribution of surface water, the planet's past climate must have been much wetter than it is today, enhancing the potential for past global habitability. Theoretical studies of Mars's ancient climate, based on assumptions of water inventory and using models of atmospheric loss, have suggested a climate that was wetter than at present but not by enough to sustain perennial lakes in topographic depressions (*4*).

The Mars Science Laboratory (MSL) mission to Gale crater, using the Curiosity rover, provides the opportunity to directly test hypotheses regarding Mars's past climate. Having discovered evidence for ancient stream and thin (meters-thick) lake deposits within its landing region (*5*), Curiosity recently explored the basal strata of Gale crater's central mountain, Aeolis Mons (informally known as Mount Sharp). Rocks that compose the foundation of this mountain include hundreds of meters of strata of unknown origin that contain evidence of hydrated minerals. We documented the succession of sedimentary rock types in this region and interpreted them in terms of past depositional processes, thereby enabling reconstructions of ancient environments and paleoclimate. In addition, we used measurements of the thickness of stratified rocks on the surface today, combined with calculations of the likely extent of crater-wall backwasting and rim erosion, to perform mass-balance calculations and infer the processes by which Mount Sharp formed.

Geologic setting

Gale crater is located on fluvially dissected highland crust along the martian topographic dichotomy boundary. Crater counts on Gale's ejecta blanket and evidence from the underlying highland crust suggest that the crater formed ~3.8 billion to 3.6 billion years ago (*6*, *7*). The interior plains of northern Gale crater (Aeolis Palus) contain remnants of eroded alluvial fan deposits and a large sedimentary mound (Mount Sharp) with the crater's central peak at its core, which may be exposed on the south side of the mound (*5*–*9*). Crater counts for Aeolis Palus suggest deposition of sedimentary materials before 3.3 billion to 3.1 billion years ago (fig. S1).

Curiosity explored two stratigraphic groups of sedimentary rocks exposed in Aeolis Palus and at the base of Mount Sharp (Figs. 1 and 2). We designate the Bradbury group as the rocks within Curiosity's landing ellipse, as well as those to the south of the ellipse, up to the contact with the Murray formation (Fig. 1). The Mount Sharp group comprises the rocks of Mount Sharp that show evidence from orbit of hydration (*10*); these include the basal Murray formation and the overlying hematite-, clay-, and sulfate-bearing units (*10*, *11*), up to an unconformity (*8*), which appears to separate rocks bearing hydrated minerals below from rocks without obvious hydrated minerals above (Fig. 1). Rover observations reveal that the mean dip of the Bradbury group is approximately horizontal, which allows elevation to be used as a surrogate for stratigraphic position in areas of poor bedrock exposure. Strata of the Bradbury group (Fig. 2) were studied along Curiosity's traverse (supplementary text) from Bradbury Landing, to the Yellowknife Bay study site, and then to the Pahrump Hills area, where the boundary between the Bradbury and Mount Sharp groups is exposed (Fig. 1). These rocks are described in ascending order.

Bradbury group sedimentology

Rocks of the Yellowknife Bay formation are composed dominantly of lacustrine mudstone and fluvial sandstone, with minor eolian sandstone (*5*, *12*). Patchy bedrock exposures between Yellowknife Bay and Kimberley become more extensive to the south of Dingo Gap (Fig. 1 shows the locations referenced in this paper), where the rover entered a set of shallow valleys with exposed rock walls and floors. These well-exposed outcrops exhibit several distinct sedimentary facies (Fig. 2).

[1]Division of Geologic and Planetary Sciences, California Institute of Technology, Pasadena, CA 91125, USA. [2]Department of Earth Science and Engineering, Imperial College London, London SW7 2AZ, UK. [3]Malin Space Science Systems, Post Office Box 910148, San Diego, CA 92121, USA. [4]Department of Earth and Planetary Sciences, University of California–Santa Cruz, Santa Cruz, CA 95064, USA. [5]Department of Geological Sciences, Indiana University, Bloomington, IN 47405, USA. [6]Department of Earth and Planetary Sciences, University of California–Davis, Davis, CA 95616, USA. [7]Jet Propulsion Laboratory, California Institute of Technology, Pasadena, CA 91109, USA. [8]Department of Earth and Planetary Sciences, Washington University in St. Louis, St. Louis, MO 63130, USA. [9]Astrogeology Science Center, U.S. Geological Survey, Flagstaff, AZ 86001, USA. [10]Center for Earth and Planetary Studies, National Air and Space Museum, Smithsonian Institution, Washington, DC 20560, USA. [11]Department of Earth and Planetary Sciences, University of Tennessee, Knoxville, TN 37996, USA. [12]Department of Earth and Planetary Sciences, Johns Hopkins University, Baltimore, MD 21218, USA. [13]Laboratoire Planétologie et Géodynamique de Nantes–Le Centre National de la Recherche, Unité Mixte de Recherche 6112 and Université de Nantes, 44322 Nantes, France. [14]Planetary Science Institute, Tucson, AZ 85719, USA. [15]Department of Geology, Western Washington University, Bellingham, WA 98225, USA. [16]Department of Space Sciences, NASA Ames Research Center, Moffett Field, CA 94035, USA. [17]NASA Goddard Space Flight Center, Greenbelt, MD 20771, USA. [18]Department of Earth and Planetary Science, University of California–Berkeley, Berkeley, CA 94720, USA. [19]Laboratoire de Géologie de Lyon, Université de Lyon, 69364 Lyon, France. [20]Department of Geology and Geophysics, Texas A&M University, College Station, TX 77843, USA. [21]Department of Physics, University of Guelph, Guelph, Ontario N1G 2W1, Canada. [22]Department of Geosciences, Stony Brook University, Stony Brook, NY 11794-2100, USA. [23]Department of Geological Sciences, University of Texas at Austin, Austin, TX 78712, USA. [24]Astromaterials Research and Exploration Science Division, NASA Johnson Space Center, Houston, TX 77058, USA. [25]Department of Geological Sciences, Brown University, Providence, RI 02912, USA. [26]Institute of Meteoritics, University of New Mexico, Albuquerque, NM 87131 USA. [27]LZ Technology, NASA Johnson Space Center, Houston, TX 77058, USA [28]Space Remote Sensing, Los Alamos National Laboratory, Los Alamos, NM 87544, USA.
***Corresponding author. E-mail: grotz@gps.caltech.edu**

In order of decreasing frequency of exposure, these include crudely stratified to cross-stratified sandstone and pebbly sandstone, conglomerate, clinoform sandstone, and finely stratified sandstone.

The crudely stratified to cross-stratified sandstones consist of poorly sorted to moderately well sorted, fine- to coarse-grained sands, with decimeter-scale sets of trough crossbeds (fig. S2). Coarser-grained beds define the base of multiple upward-fining sequences. Poorly sorted pebble-rich sandstones also are common. Pebbles are dispersed throughout the sandstone framework, reach up to ~22 mm in diameter, and are subangular to subrounded in shape (*12*). The facies is grain-supported but shows no preferred grain orientation. Elongate fine-grained clasts may be mudstone intraclasts (fig. S2).

The conglomerates are interstratified with sandstones and pebbly sandstones (*12*, *13*) and are present throughout the Bradbury group. Characteristically, they are weakly stratified, poorly sorted, and composed of angular to subrounded clasts (fig. S2) that reach up to 6 cm in diameter. Beds of conglomerate are 10 to 30 cm thick.

The presence of grain-supported sandstones and pebbly sandstones and the common occurrence of cross-stratification provide strong evidence for bedload sediment transport in an ancient fluvial system. We also interpret the conglomerates as evidence of deposition in a fluvial environment, formed by the migration of subaqueous bedforms or barforms, similar to conglomerates observed between Bradbury Landing and Yellowknife Bay (*13*). The low-to-moderate level of rounding is consistent with a short transport distance, such as deposition in an alluvial fan environment.

Finely stratified sandstones occur rarely in the Bradbury group and are characterized by regular millimeter-scale laminae that form thin sheets 5 to 10 cm thick and, rarely, dune-scale cross-stratification. In one case, the fine laminae that make up the foresets of a small dune are themselves cross-stratified (fig. S2), indicating centimeter-scale compound cross-stratification. The fine regular lamination is similar to "pinstripe" lamination, which is produced by the migration of eolian impact ripples (*14*).

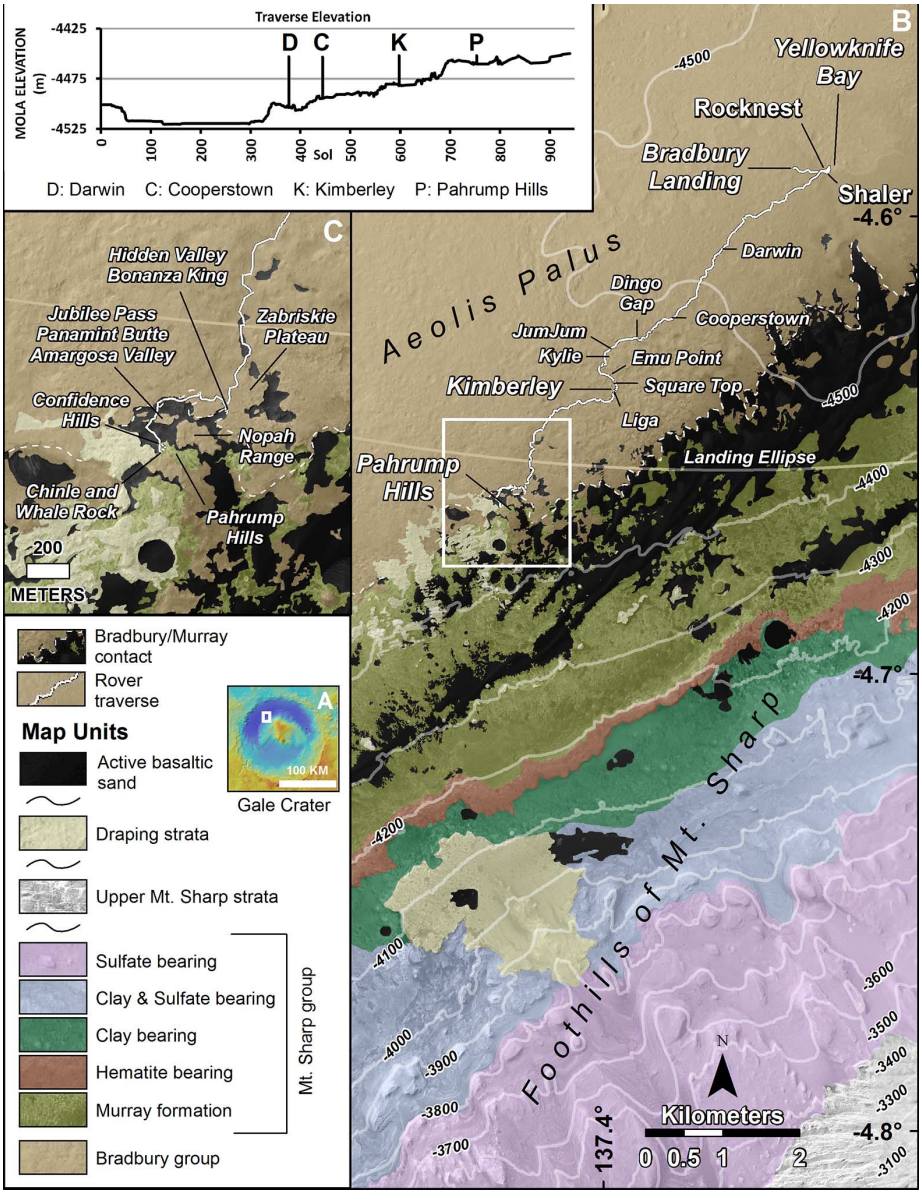

Fig. 1. Regional geologic map showing the location of the rover traverse and key study areas. Inset map (**A**) shows Gale crater topography; the white box outlines the area shown in (B). (**B**) Geologic map showing the principal stratigraphic units exposed at Aeolis Palus and the foothills of Mount Sharp, the major study locations, the rover traverse, and the landing ellipse. The white box outlines the area shown in (C). (**C**) Map details and locations of study points in the vicinity of Pahrump Hills. (Top inset) Topographic profile of the rover traverse.

Clinoform sandstones

An unusual texture, characterized by distinct striations and here termed "orbital striated outcrop" (OSO), is observed in images collected by the High Resolution Imaging Science Experiment (HiRISE) orbiter (Fig. 3A). The OSO texture is exposed within dissected parts of southern Aeolis Palus (Fig. 3B) and is typified by striations consistently trending east by northeast–west by southwest (trend direction of N65°E) that extend up to ~100 m along strike within individual outcrops. The OSO is exposed discontinuously in topographic lows that reflect partial exhumation from beneath overlying strata (supplementary text). These exposures of OSO are distributed over an area ~3 km in the east-west direction and ~2.5 km in the north-south direction (Fig. 3B). Striations are expressed in HiRISE images as alternating bands with light-dark albedo variations (Fig. 3A).

Rover observations relate the OSO texture to sedimentary rocks with distinctive geometries, known as clinoform sandstones (Fig. 4). Clinoforms are inclined stratal surfaces, found within volumes of sediments and sedimentary rocks, that occur over a wide range of spatial scales and depositional settings (*15*). Typically, they comprise a low-gradient topset that transitions into a steeper-gradient foreset zone, which may transition into low-gradient bottomsets. They are distinct from crossbedding in that they are larger in scale, with planar to sigmoidal (rather than trough-shaped) foreset geometry, and have a consistent dip direction when measured over kilometer-length scales (*16*).

Rover observations of the OSO show clinoform geometries that dip 10° to 20° to the south. In addition, rover observations of valley walls reveal clinoform sandstones that cannot be observed from orbit. Observations of the upper and lower bounding surfaces of these inclined sets of strata show that the clinoforms range from 1 to 4 m in thickness.

Observations of the clinoform sandstones at the north Kimberley "Square Top" target show that they are composed of fine sands with dispersed coarser grains (Fig. 4C). The latter are subangular to rounded, coarse to very coarse grains, with

the larger grains ranging from 0.5 to 3.1 mm in diameter and with an average grain diameter of 1.0 to 1.4 mm. An underlying conglomerate bed contains subangular to subrounded grains up to 3 mm in diameter. Farther south, inclined, interstratified granule- and pebble-rich beds and sandstone beds marked by poorly sorted, subangular to subrounded grains are present (Fig. 4D). The largest grains at the "Liga" target are 3.1 to 4.7 mm in diameter. Such coarse grain sizes indicate transport by water rather than by wind.

Recessive and probably poorly cemented dipping conglomerates are interstratified with resistant, well-cemented sandstones at Kylie and Kimberley (Fig. 4C). The repetition of beds with different resistances to erosion may result from differential cementation of beds with different grain sizes. Beds that form clinoform foresets are massive to poorly stratified, suggesting emplacement on foreset surfaces via downslope grain flows.

Only a few complete exposures of clinoforms are observable, and these have sigmoidal geometries (*17*), in which gently dipping topset beds steepen and transition into south-dipping foreset beds that become shallow at their bases. A distinct transition from topset to foreset geometry is apparent at the north end of the Kimberley outcrop.

More generally, the foreset beds are truncated at their tops by erosional surfaces capped by subhorizontal strata (Fig. 4B). These truncating strata have variable characteristics that probably reflect different formation processes. In places, these strata appear to be coarser-grained sandstones and conglomerates, which we interpret as fluvial topsets. Elsewhere, these truncating strata are fine-grained, thin-bedded sandstones with small-scale cross-stratification, probably also of fluvial origin. Locally, bedsets of small-scale cross-stratification with northward paleoflow indicators suggest eolian reworking of previously deposited fluvial sands.

Exposures of OSO rise in elevation from −4502 to −4460 m from north to south (Fig. 3C), which indicates that clinoform sandstones also should occur at stratigraphically higher levels to the south, toward Mount Sharp. When compared with the elevation of clinoform sandstones observed at Kylie, rover observations confirm that south-dipping clinoform sandstones occur ~10 m higher at Kimberley, ~25 m higher at Zabriskie Plateau and in Hidden Valley, and ~30 m higher in the southwest arm of Hidden Valley.

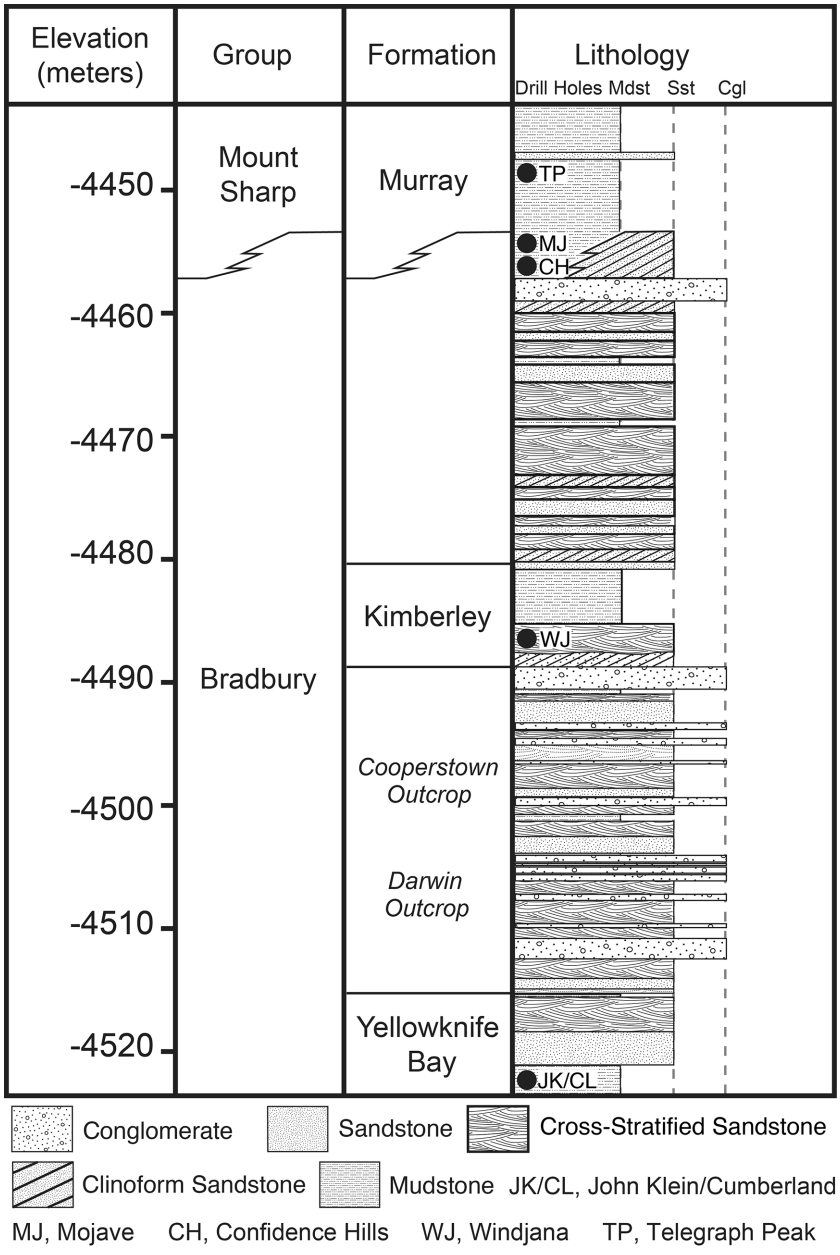

Fig. 2. Stratigraphic column for the sedimentary facies from Yellowknife Bay to Pahrump Hills. The contact between the Bradbury group (Aeolis Palus) and the Mount Sharp group (Aeolis Mons) is marked by interfingering of facies. Mdst, mudstone; Sst, sandstone; Cgl, conglomerate.

Synthesis: Reconstructing ancient deltas

The consistent strike of the OSO clinoform sandstones across hundreds of meters (in map view) and the presence of consistent south-dipping beds (observed in cliff-face sections) tightly constrain the mode of deposition for these sandstones. On Earth, inclined foresets of sand and gravel can be deposited by migrating river dunes, river bars, and delta mouth bars. In each case, inclined foresets are produced by sediment accretion at the margins of depositional bedforms. Fluvial barforms, such as scroll bars, are curved in the strike direction at scales of tens to hundreds of meters, because they reflect the growth of point bars in meandering river systems (*18*–*20*). Moreover, planform shapes of bars vary spatially from one bar to another (*20*, *21*). Similarly, bars in braided rivers show complex patterns of sediment accretion, with bar growth and inclined strata development both downstream and at the lateral margins of bars (*22*–*24*). The absence of marked curvature in the OSO striations, both within outcrops and across the ~2- to 3-km outcrop belt, rules out river bars as an interpretation of the clinoform sandstones.

The migration of fluvial and eolian transverse dunes can produce large-scale patterns of inclined bedding in sands (*25*–*27*). In this scenario, striations observed in map view would represent intersections of dune lee deposits with the surface. It is unlikely that transverse dunes could maintain such linear striation trends over an along-strike distance of several kilometers. Transverse dunes typically evolve into structures with considerable sinuosity in their crest lines, and hence they produce foresets with variable dip azimuths (*28*–*30*). Even linear dunes typically have planform sinuosities and superimposed bedforms or other features that produce variable dip azimuths where the dunes migrate laterally (*27*). Furthermore, the migration of dunes produces erosional truncation surfaces that separate sets of climbing dunes. The absence of such surfaces suggests that migrating bedforms, either eolian

or fluvial, were not responsible for clinoform development in the OSO strata.

Our favored interpretation is that the clinoforms represent deposition at small deltas where braided river mouths entered a body of standing water (*31*, *32*). As a river flows into standing water, sediment transport capacity and competence abruptly decrease, leading to deposition and the formation of deltas (*33*). Progressive accretion of sediment leads to the formation of inclined foresets dipping systematically in one direction. Thus, we interpret the south-dipping foresets of the clinoform sandstones to result from the southward advance of deltas fed by streams from the crater rim to the north (Fig. 3, D and E). The limited spread in the trend of delta foresets differs from that of younger terrestrial alluvial systems, which are characterized by a wider spread in the orientation of terminal distributary channels (and thus foresets) due to mud deposition and bank stabilization aided by vegetation (*34*, *35*). However, it is consistent with alluvial landscapes on Earth before the advent of bank-stabilizing vegetation. For example, the Precambrian stratigraphic record shows evidence for the coalescence of individual delta lobes to form a broad complex that might have an arcuate shape across tens of kilometers, but that has an approximately linear delta front at a scale of 100 m to a kilometer (*36*, *37*). A relatively narrow spread of paleocurrent indicators in distal fluvial facies is consistent with relatively straight shorelines on the Precambrian Earth (*38*–*40*). For these older landscapes, which make better analogs for fluvial sedimentation on Mars, the trend of clinoforms would show a narrow dispersion, similar to the martian clinoforms.

This interpretation predicts that southward (downstream), in the region marked today by the lower slopes of Mount Sharp, fluvial-deltaic deposits should undergo a lateral facies transition into fine-grained lacustrine deposits. The southward rise in clinoform elevation can be explained in this context (Fig. 3E). Because they were formed at deltas, the tops of clinoforms represent lake-level elevation, and so the occurrence of the clinoforms at progressively higher elevations requires a net lake-level rise. The clinoforms' small size (a few meters) suggests that water depths at the sites of their development were not deeper than a few meters to a few tens of meters; this would have required substantial infilling of the Gale crater lake basin with sediment, thus leading to aggradation of the fluvial system, in addition to progradation. We propose that large-scale progradation and aggradation of the fluvial system, concomitant with basin infilling, led to the systematic stratigraphic rise of multiple clinoform units (Fig. 3D, E). Clinoform outcrops at different elevations do not represent the same stratal unit but rather distinct units that were stacked during fluvial progradation, which is also commonly the case in terrestrial fluvial-lacustrine deposits (*41*).

The discovery of deltaic deposits in ancient strata that represent sediment progradation toward Mount Sharp changes the way that we think about its development. Although the modern landscape dips northward away from Mount Sharp, these ancient sedimentary deposits indicate that a basin once existed where today there is a mountain.

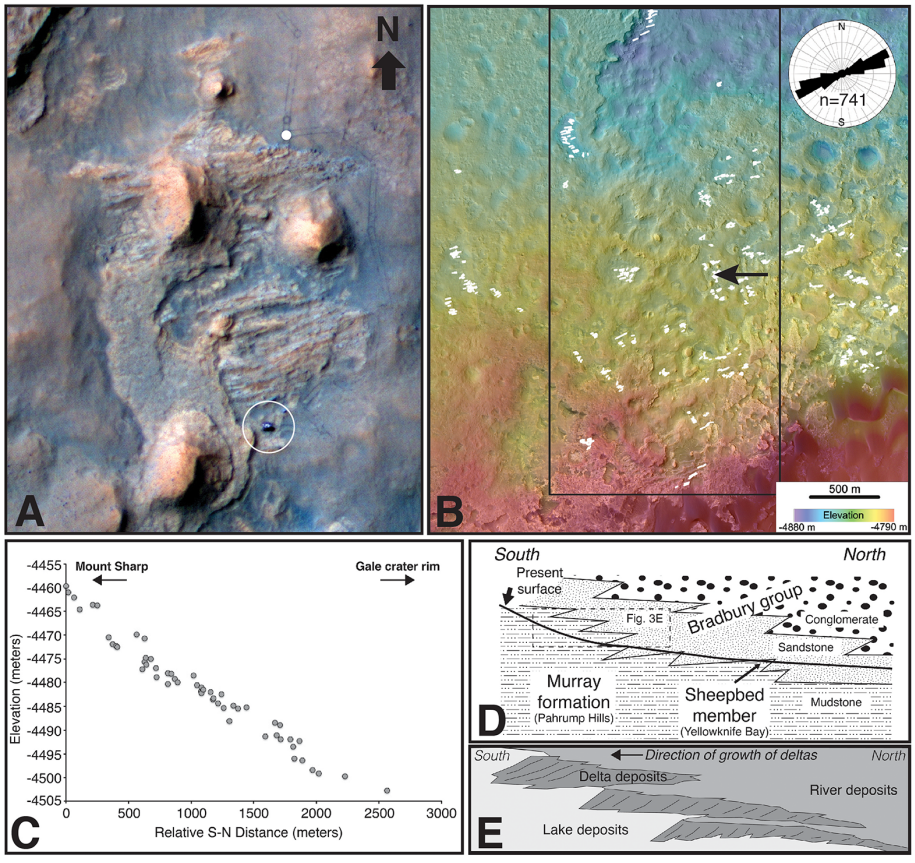

Fig. 3. Occurrence of OSO. (**A**) OSO as observed in HiRISE image ESP_036128_1755. For scale, the Curiosity rover (circled) is 2.9 m long. The white dot shows the viewpoint for the image in Fig. 4A. (**B**) Topography of a portion of Aeolis Palus with plotted occurrences of OSO (in white), which rise in elevation to the south. The orientation of striations observed at all mapped localities (inset rose diagram) shows a preferred northeast-southwest orientation; this trend is approximately normal to the inferred south-southeast fluvial paleoflow direction. The box indicates the area sampled to create (C). The black arrow indicates the Kimberley outcrop shown in (A). (**C**) The southward rise in OSO elevation. Average elevation data for each mapped occurrence within the box in (B) were collapsed onto a single line at the center of the box, and their elevation values were plotted as a function of distance along that line. (**D**) Facies transition from conglomerate to sandstone to mudstone, in cross section, relative to the rover traverse. This rise in elevation is consistent with rover data; initially, the rover drove uphill across exhumed fluvial facies, then crossed a boundary into deltaic facies (Kimberley region), and ultimately crossed into time-equivalent lacustrine facies (Murray formation at Pahrump Hills). (**E**) Facies transition from alluvial to deltaic to lacustrine, in cross section, with stacked deltaic clinoforms similar to those observed in Bradbury group. Such facies changes are common on Earth for similar environments but require infilling of the basin at the same time as deltaic progradation occurs.

The relationship between the Bradbury group and the Murray formation

The contact between the Bradbury group and the Murray formation was explored in the valleys that extend from Hidden Valley to the Pahrump Hills (Fig. 5). The Murray formation is a fine-grained laminated mudstone, based on Mars Hand Lens Imager (MAHLI) observations collected where Curiosity drove into Hidden Valley. This fine-grained, finely laminated facies is overlain by a thickly laminated sedimentary facies with distinctively even layering (Fig. 6). The thickly laminated facies is interstratified with thin-bedded sandstones and is ultimately overlain by crossbedded or clinoform sandstones. Observations of other valley walls show that similar systematic progressions of facies occur at different elevations, with a southward rise in the crossbedded and clinoform sandstones (Fig. 5). We interpret this systematic variation to represent north-to-south interfingering of the coarser, fluvial-deltaic facies of the Bradbury group with the finer-grained facies of the Murray formation. This is consistent with a downstream termination of fluvial influence related to alluvial fans prograding southward from the northern Gale crater rim. In bulk, the Murray formation

is believed to overlie the Bradbury group as shown in Fig. 2; however, near the contact, the two units interfinger, so that the Bradbury group locally overlies the Murray formation in the Hidden Valley–Amargosa Valley area.

Interfingering of the Bradbury group and the Murray formation is additionally supported by observations collected farther to the southwest (Fig. 5). Southward-dipping clinoform facies occur in several locations: the entrance to Amargosa Valley at Jubilee Pass, the eastern wall of the Nopah Range, and the northern margin of Panamint Butte. The latter locality is notable in that fine-grained, recessive deposits of the Murray formation directly overlie coarser-grained, south-

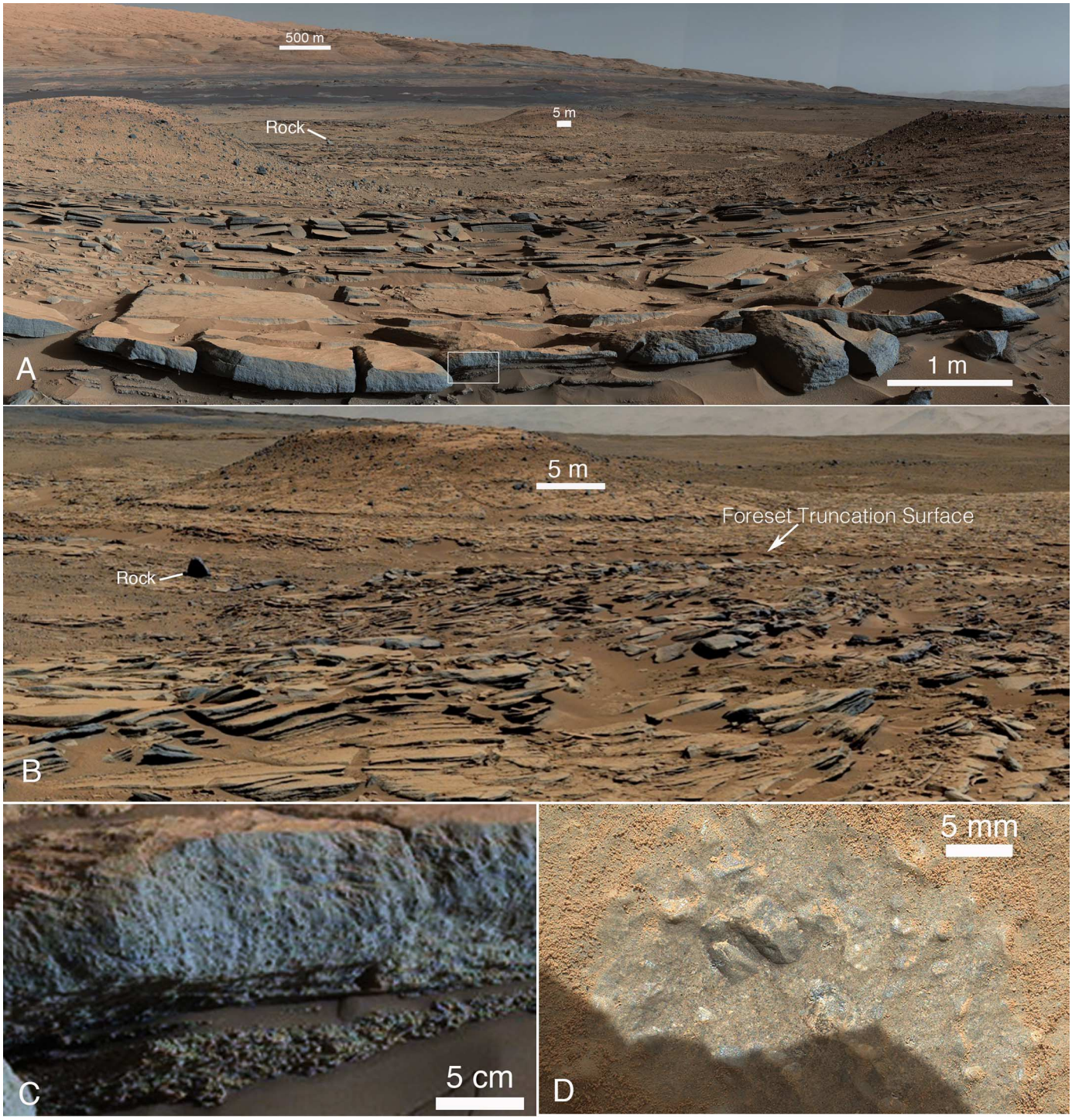

Fig. 4. Clinoform sandstones. (**A**) OSO at Kimberley; the view is to south and shows south-dipping clinoform facies. The viewpoint is represented by the white dot in Fig. 3A. The box indicates the area shown in (C). "Rock" indicates same feature as in (B) for orientation. The Mastcam image was acquired on martian day (sol) 580. (**B**) Westward view of the same south-dipping clinoform sandstones in (A). The clinoforms emerge from beneath overlying strata to the west, exposed at a small butte (the scale bar is placed on this feature). The Mastcam image was acquired on sol 590. (**C**) Coarse grain size of the clinoform facies. The Mastcam image was acquired on sol 674, at the Square Top locality shown in (A). (**D**) Close-up of coarse grains observed in clinoform facies at Liga, ~2 m north of the rock indicated in (A) and (B). MAHLI focus merge product 0601MH0003810000203227R00.

dipping clinoform sandstones and conglomerates (fig. S5). The direct juxtaposition of fine- and coarse-grained sediments along a south-dipping contact is strong evidence for the coeval deposition of the Bradbury group and the Murray formation.

Further insight is provided by comparing the two bodies of rock as a function of elevation. Over short distances within the valley system, the two units vary and can be equivalent in elevation. The existence of Bradbury group rocks, including clinoform facies, at the same elevation as laminated mudstone facies of the Murray formation (Fig. 5) suggests temporal equivalence. Alternatively, the rocks might be in unconformable contact; if so, the Bradbury group would be the younger of the two and would have to abruptly abut the Murray formation. That relationship would impose substantial constraints on the sediment dispersal represented by Bradbury alluvial fans; the generally southward paleoflow would have to deflect abruptly to either easterly or westerly flow over a short runout distance of less than 100 m. No evidence for this is apparent in the observed sediment transport directions, including the dip of the clinoform sandstones. Therefore, although an abrupt unconformable contact cannot be completely discounted because of intermittent outcrop exposure, the simplest interpretation is that the facies interfinger over a scale of 50 to 100 m, which is characteristic of fluvio-lacustrine settings (*42*). In this case, timelines (stratal surfaces) in the clinoform facies, such as those in the Nopah Range section (Fig. 5), would transition along the inferred paleodepositional slope into mudstones of the Murray formation, exposed at the Pahrump Hills outcrop.

The Murray formation in the Hidden Valley–Pahrump Hills region

After passing through Amargosa Valley, Curiosity arrived at the Pahrump Hills outcrop (Fig. 5). This and smaller outcrops along valley walls constitute the northernmost exposures of the Murray formation, which orbital data suggest extends southward to the hematite-bearing ridge (*11*) that overlies it in the Mount Sharp group (Fig. 8). Given the rise in elevation from north to south, and assuming subhorizontal bedding, we infer a stratigraphic thickness for the Murray formation of ~150 m between Hidden Valley and the hematite-bearing ridge. The Pahrump Hills section is estimated to be ~13 m thick (Fig. 7A), thus exposing the lowermost ~10% of the formation. (This does not apply to older strata in the subsurface that might be genetically related to the Murray formation.)

Observed in HiRISE image data, the Murray formation has a homogeneous appearance, in part due to the absence of detectable stratification in images with meter-scale resolution. However, Curiosity image data show that the Murray formation is stratified at the millimeter scale, fine-grained, and exposed in dust-covered outcrops; these attributes promote the uniform appearance observed in HiRISE data.

Four sedimentary facies are recognized within the Murray formation outcrops exposed between Hidden Valley and Pahrump Hills. These include thinly laminated mudstone, thickly laminated mudstone-siltstone, cross-laminated sandstone, and conglomerate. All are exposed at the Pahrump Hills outcrop, where the section begins with conglomerate and is overlain by finely laminated, fine-grained mudstone with a single intercalated bed, 20 to 30 cm thick, of medium-grained, centimeter-scale cross-laminated sandstone (Whale Rock). The top of the outcrop is capped by thickly laminated facies, and massive gray sandstones occur farther uphill, forming a capping unit. The Pahrump Hills outcrop is the reference section for the basal part of the Murray formation, and these rocks, which are broadly exposed in the Hidden Valley–Amargosa Valley system, are designated the Pahrump Hills member (Fig. 7A). Early to late diagenetic textures are also present (supplementary text), including dendritic concretions, prismatic crystal pseudomorphs, and calcium sulfate–filled fractures (fig. S3)

Conglomerate is exposed at the base of the section at Pahrump Hills. Based on the conglomerate's

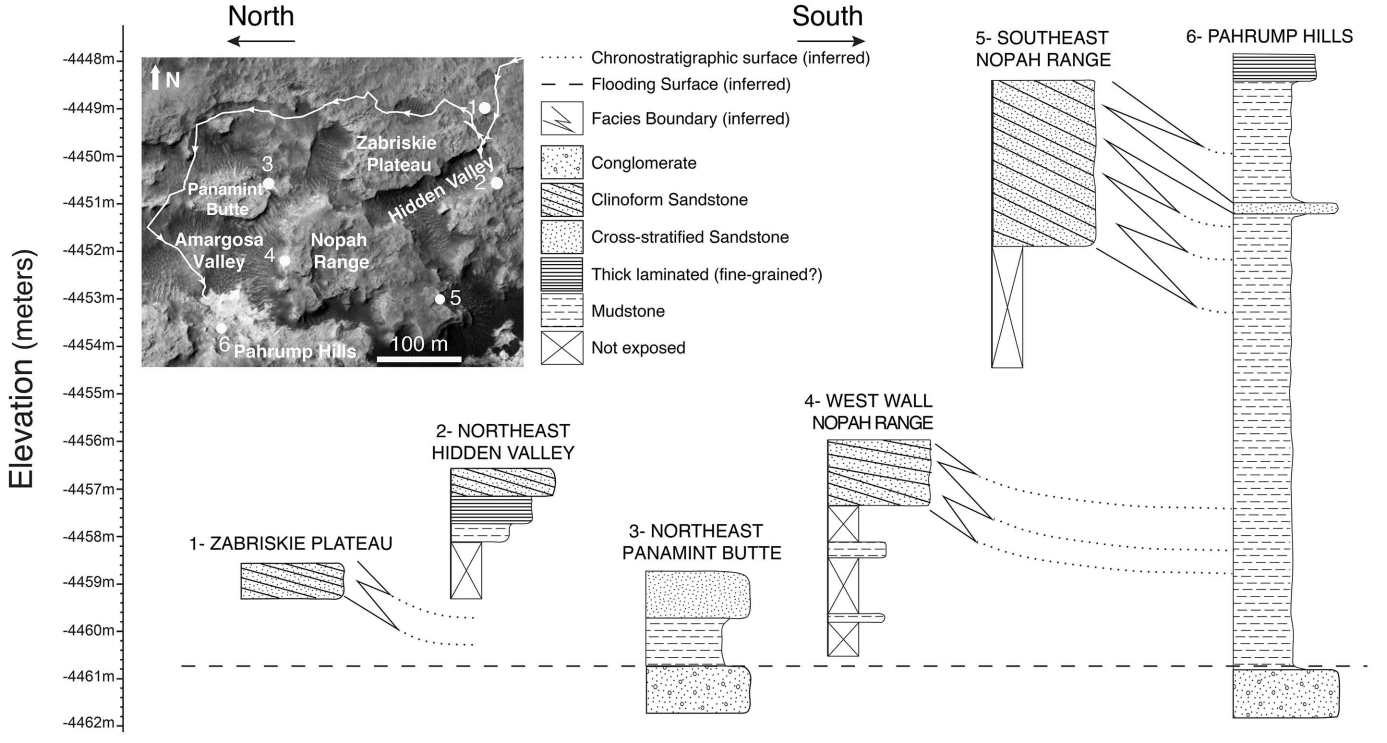

Fig. 5. Facies relationships at the contact between the Bradbury group and the Murray formation. Laminated mudstones are exposed at Pahrump Hills (section 6). Elevation data indicate that these the Bradbury group and Pahrump Hills section could be time-equivalent. The elevations of south-dipping facies in the northerly sections (1 to 5) are lower than those of the mudstones at Pahrump Hills. In Hidden Valley (section 2), laminated mudstones are overlain by what appears to be a gradational, upward-coarsening sequence that culminates in crossbedded sandstones of fluvial origin (Fig. 6). The lateral transition from coarse-grained fluvial and deltaic facies to fine-grained lacustrine facies is a prediction of the fluvio-lacustrine facies association. This is supported by direct observations at Panamint Butte and Pahrump Hills (sections 3 and 6), where Mastcam data show mudstones overlying conglomerate and sandstone facies. At Panamint Butte, mudstones overlie south-dipping sandstone and conglomerate facies, as shown in fig. S4.

distribution across Jubilee Pass, Panamint Butte, and Pahrump Hills, we infer that it underlies the thinly laminated mudstone facies. This relationship is particularly evident at Panamint Butte (fig. S4). At Pahrump Hills, thinly laminated mudstones overlie and drape depositional topography over the conglomerates.

Finely laminated mudstone is the dominant facies at Pahrump Hills (Fig. 7B). It is also exposed at the Bonanza King outcrop, located along the northeastern side of Hidden Valley. Our analysis constrains the grain size of this facies to be below the 60- to 70-μm limit of resolution (table S1), confirming its classification as mudstone (*43*). "Mud" is used here in the nongenetic sense, not necessarily implying wetness, and represents only a grain-size designation for which the large majority of particles are below 62.5 μm (*43*). Stratification of the finely laminated mudstone facies is prominent throughout much of the section (Fig. 7A). Image analysis of representative stratification (supplementary text) shows that the mean lamina thickness is ~2.2 mm (figs. S4 and S5 and table S2). The lamination is characteristically parallel, with a horizontal to gently inclined attitude; individual laminae exhibit high lateral continuity of at least several tens of centimeters. An exception to this occurs at the Chinle outcrop, where low-angle truncation surfaces are overlain by laminae that conform to the geometry of the truncation surface. Laminae forming the finely laminated mudstone facies lack evidence of ripples, cross-stratification, or even low angles of climb. Furthermore, no evidence of sediment-filled mudcracks or of intraclasts, which would indicate reworking of muds by currents, is apparent. Additionally, outsized clasts are absent.

The thickly laminated facies is similar to the finely laminated mudstone facies, but it has a characteristically greater lamina thickness (Fig. 7C). This facies occurs along the walls of Hidden Valley at higher elevations, between the finely laminated mudstones and the overlying capping sandstones. It also occurs toward the top of the Pahrump Hills section. It has not been examined by MAHLI, so its grain size is not known; however, Mast Camera (Mastcam) images suggest that it is fine-grained. Image analysis shows that its laminae have a mean thickness of 5 mm, double what was measured in the finely laminated mudstone facies (fig. S5 and table S2). Along the northwest-facing wall of Hidden Valley, the thickly laminated facies is overlain by thicker beds with a more resistant weathering profile, and ultimately by thick-bedded, trough–cross-stratified sandstone (Fig. 6), constituting a thickening-upward succession. There is some evidence that the thickly laminated facies may also transition laterally into thicker, more resistant beds, suggesting coeval deposition.

Cross-laminated sandstone in a single laterally discontinuous bed makes up the Whale Rock outcrop (Fig. 7D). The bed is 30 to 40 cm thick and forms a lens within the overall fine-grained Pahrump Hills stratigraphy. Grains are moderately well sorted and rounded, and the mean grain size is ~0.6 mm, reaching up to ~0.8 mm. Ripples on Earth generally are composed of finer-grain sediments and only uncommonly include the grain sizes observed in this outcrop. However, for Mars, the ripple stability field expands to include sizes up to 1.3 mm (*44*). Cross-laminae form bedsets a few centimeters thick, with subcritical angles of climb and apparent southeastward paleocurrent (sediment transport) directions. Several other laterally discontinuous, cross-stratified sandstone beds, also forming lenses, are present at approximately the same stratigraphic level, west of the Whale Rock outcrop. These lenses are all 2 to 4 m in width and a few tens of centimeters in thickness. Trough crossbedding is visible in Mastcam images. The lenses are spaced 5 to 7 m apart.

Synthesis: Reconstructing an ancient lake

Our preferred interpretation for the Murray formation, as it is exposed in the Pahrump Hills area, invokes predominantly subaqueous, lacustrine sedimentation adjacent to a fluvial-deltaic complex. This best explains the attributes of individual facies and the collective assemblage of facies, and it is supported by the broader context of the Bradbury group sedimentology and stratigraphy. The key elements of this model are as follows: (i) The finely laminated mudstones are interpreted as distal deposits related to sediment plumes discharging into a body of standing water, whereas the thickly laminated facies are more proximal equivalents; (ii) the thickening-upward sequence observed in Hidden Valley and at the top of the Pahrump Hills section represents fluvial-deltaic progradation over coeval lacustrine deposits; and (iii) the sedimentology of the facies in the Bradbury group, in particular the clinoform sandstones, predicts the presence of down-gradient lacustrine equivalents in a more southerly paleogeographic position, thus providing a plausible genetic tie between the Bradbury group and the Mount Sharp group.

The finely laminated mudstone facies, considered jointly with the thickly laminated facies,

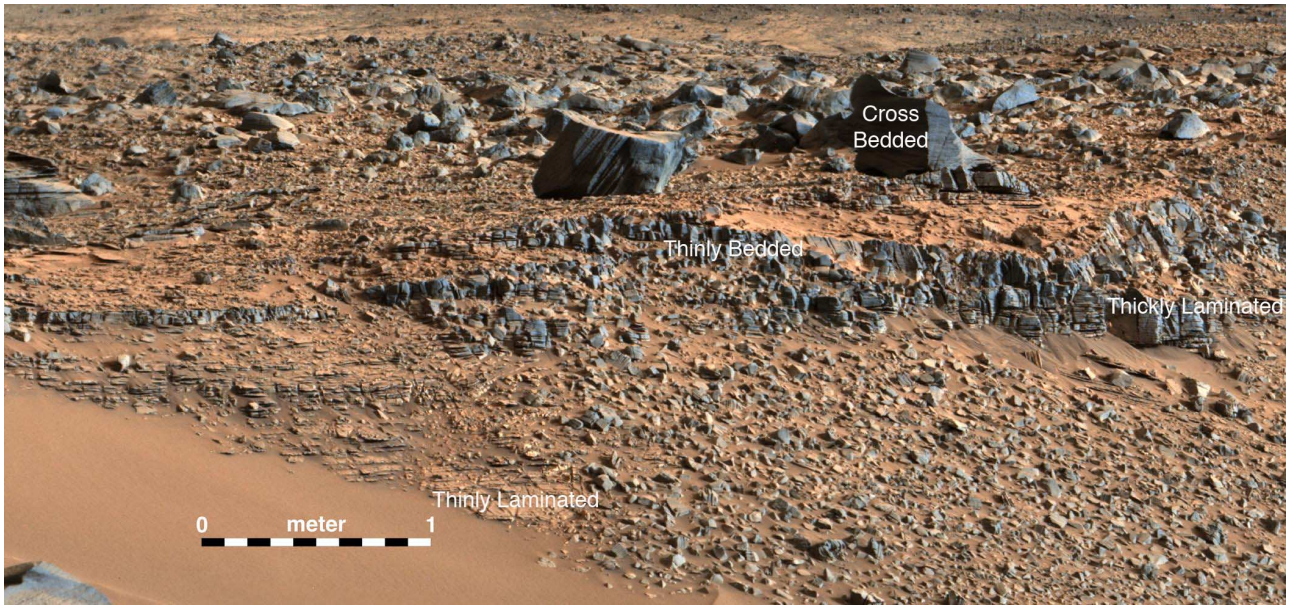

Fig. 6. Stratigraphy of the southeast wall of Hidden Valley. The inset map in Fig. 5 shows the location of Hidden Valley. Finely laminated mudstones exposed at lower elevations grade upward into thickly laminated facies, then into thinly-bedded resistant facies, and ultimately into abundant loose blocks of crossbedded sandstone. Strata of the thin-bedded interval appear to transition laterally into the more recessive laminated mudstones. Although the crossbedded facies at this location is represented by blocks, the blocks can be traced laterally into continuous bedding just a few tens of meters away. This succession is most simply interpreted as a lacustrine facies overlain by laterally prograding fluvial-deltaic deposits.

represents either hyperpycnal or hypopycnal sediment flows (*45*). Hyperpycnal flows are gravity-driven, slope-hugging currents in front of a delta, which result from the excess negative buoyancy of the discharging sediment plume relative to the ambient lake water. In the hypopycnal case, the plume is positively buoyant and extends across the surface of the lake, until flow expansion diminishes its momentum, resulting in deceleration to the point at which gravity-driven settling drives particles downward through the water column. Thin lamination with regular spacing and substantial lateral continuity is consistent with either mechanism. For moderate-sized rivers, either flow type would create a deposit that thins distally over scales of a few hundred meters (*46*), thus explaining the difference in lamina thickness between the two facies.

The general absence of coarser graded beds, or beds with flow-deceleration sequences, suggest that deposition may have occurred dominantly by hypopycnal flows. However, the lens-shaped cross-laminated sandstone bodies (Whale Rock and the laterally adjacent sandstones) could be gullied delta foreslope deposits. Their limited east-west extent suggests a north-south elongation of sandstone bodies that is in turn consistent with the general southward transport direction observed throughout the Bradbury group. The climbing-ripple cross-stratification at Whale Rock supports sediment transport under decelerating flow conditions, such as those that might occur in a bottom-hugging sediment gravity flow. Alternatively, these sandstones might represent fluvial deposits incised into a drying lake bed.

The finely and thickly laminated facies show repeating characteristic lamina thicknesses, similar to varves observed in glacial lake sediments (*47*). Although the grain size is too fine to confirm, the accentuation of the Pahrump Hills laminae by weathering may be due to repeating differences in grain size, porosity, composition, or grain orientation; such variations may reflect the characteristic time scales of a range of local processes, including the production and delivery of detrital sediment from the catchment area, or precipitation of authigenic materials from the overlying water or within the sediments. Pro- and periglacial lakes on Earth typically develop varves that reflect a combination of seasonal variation in each of these processes. Varves record strong physical weathering in sediment-source regions and where sediment fluxes are driven by seasonal changes in runoff (*48*). Varves are typically normally graded, and fine particles may reflect the waning stages of hyperpycnal flows or deposition from suspension during intervals when ice covers the water column and prevents wind-driven turbulence. Lamina thicknesses in the Pahrump Hills section are similar to those in fluvial-deltaic depositional systems on Earth (*49*); consequently, they are consistent with our hypothesis that these laminae record events of distal sediment fallout in a lacustrine setting in the down-dip part of a fluvial-deltaic system.

Alternative mechanisms for the deposition of the mudstone involve eolian processes, including the settling of dust or fine volcanic ash from the atmosphere and traction transport of sand and silt. Wind-blown dust (loess) or ash may constitute some fraction of the sediment in the basin but, if so, the particles are likely to have settled through water. Loess and ash are both characterized by massive bedding, rather than fine lamination, when deposited from the atmosphere (*50*, *51*); the grain-size segregation necessary to create lamination is far more likely to occur if the sediments settle in water. Furthermore, deposition of airborne fine grains cannot explain the regular thickness of the layers or the thinning between the thickly and finely laminated facies. Therefore, we exclude the settling of fine grains directly from the atmosphere as a primary sediment accumulation mechanism.

The observed parallel stratification is not typical of either dry eolian dunes or wet interdunes (*52*). Flat beds do occur in eolian sandstones, but they generally do so in sets that are a few tens of centimeters thick [and not greater than ~2 m (*52*)] and are typically interbedded with or grade upward into eolian crossbeds. The sets of flat beds at Pahrump Hills are much thicker and, more importantly, crossbeds with eolian stratification resembling bottomsets and foresets in sandstones on Earth (*52*, *53*) were not observed.

A final set of possible mechanisms includes the formation of eolian impact ripples, "adhesion

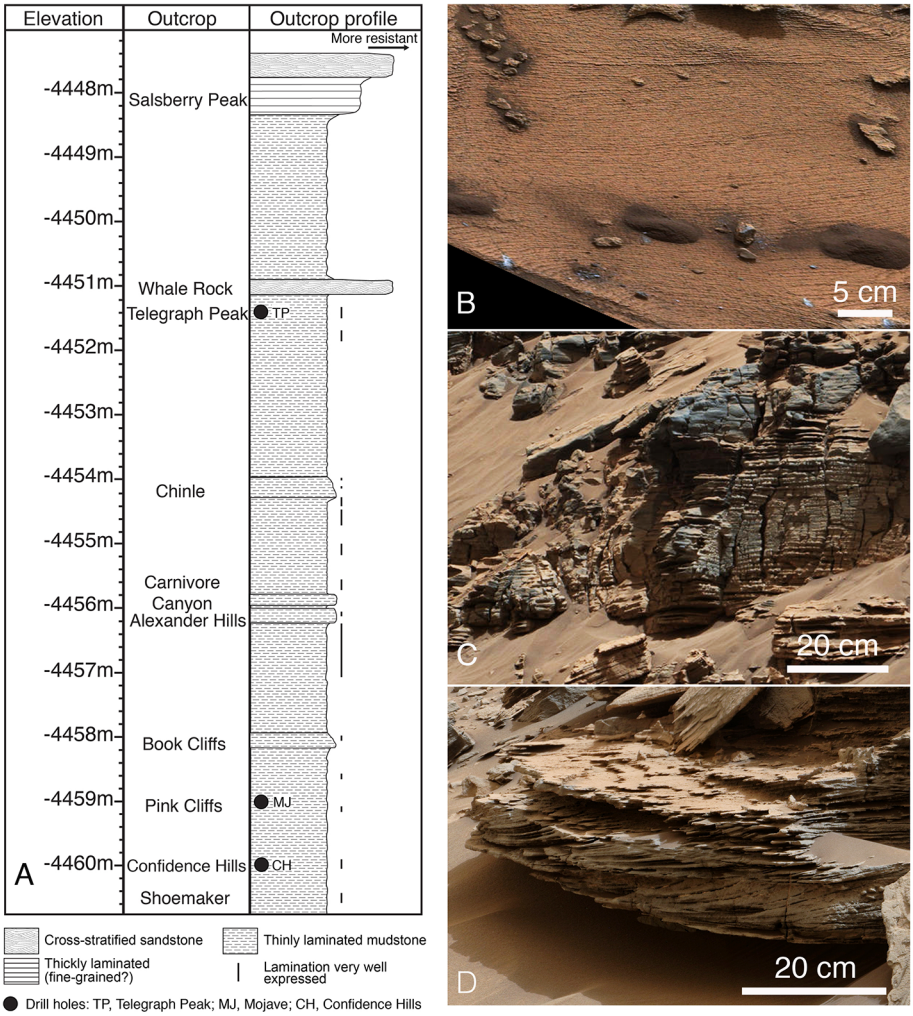

Fig. 7. Stratigraphy and facies of the Murray formation at Pahrump Hills. (**A**) Mastcam images show that the entire outcrop is finely laminated; in some positions, this texture is particularly well expressed as a result of wind-induced etching and the absence of dust. More resistant intervals probably result from differential cementation. The thinly laminated mudstone has a gradational contact with the overlying thickly laminated facies, which in turn is overlain by cross-stratified sandstone. This thickening- and coarsening-upward sequence mimics that seen in Hidden Valley (Figs. 5 and 6). Whale Rock is an intercalated sandstone lens. (**B**) Finely laminated mudstone (Mastcam image acquired on sol 792). (**C**) Thickly laminated facies (Mastcam image acquired on sol 712). (**D**) Cross-laminated facies observed at Whale Rock, formed by flows in a southeastward direction that created climbing-ripple cross-stratification (Mastcam image acquired on sol 796).

ripples," and "adhesion lamination;" however, the textures of these features are distinctly different from the lamination observed at Pahrump Hills and are thus discounted (supplementary text).

Exhumation and formation of Mount Sharp

The geologic constraints described above require a major exhumation event as part of the origin of Mount Sharp. Between Yellowknife Bay and Pahrump Hills, Curiosity drove uphill across 75 m of exposed stratigraphy. The fluvial sediments of the Bradbury group, derived from the northern crater rim, were once part of a laterally extensive succession of strata that has been eroded and exhumed (Fig. 8). The net southward transport directions, as well as the north-to-south transition between facies, imply that outcrops of the Bradbury group are erosional remnants of an alluvial plain that stood at least 75 m above the current elevation of Yellowknife Bay, extending southward from the northern crater rim. Furthermore, if the Murray formation is the distal facies equivalent of the Bradbury group, and the Murray formation continues uphill to its contact with the hematite-bearing ridge identified in orbiter data (Fig. 1), then it is possible that those rocks at higher elevations also had northern fluvial equivalents that extended to the crater wall (Fig. 8B). In this case, at least hundreds of meters of erosion would be required to create the topography that is observed today. We therefore interpret the Aeolis Palus surface, and at least the lower part of Mount Sharp's surface, to be erosional in origin, as represented by the dashed line in Fig. 8.

We suggest the following history as an explanation of our observations: After the formation of the crater and the simultaneous creation of a moat between the rim and the central peak, sediments were supplied via erosion and degradation of the northern wall and central peak (Fig. 8B). Fluvial sediments were deposited along the topographic gradient toward the center of the moat, where a time-equivalent lacustrine facies was deposited. This history is captured in the transition observed between the Bradbury group and the Murray formation (Fig. 1). Deposition of the complete Murray formation then occurred, followed by the hematite-bearing ridge unit, the thin clay mineral–bearing unit, and ultimately a thicker section of sulfate-dominated strata that extends upward to an unconformity, which separates hydrated strata from overlying, apparently anhydrous strata (Fig. 1) (*10*). The origin of these units is not well known yet, because they have been observed only in data acquired from orbit, but all have interacted with water, and all are assumed to be time-equivalent with the erosion and backwasting of the northern wall and central peak. The unconformity may record a marked change in climate, indicated by the upper strata, a thick sequence of possibly eolian facies (Fig. 8C) (*10*, *54*).

The emplacement of several kilometers of sediment above the Murray formation would have compacted it and any underlying sediments that are currently beneath the surface of Aeolis Palus (supplementary text). Sediment compaction would have differentially affected the fine sediments of the Murray formation, including those in the subsurface (fig. S7). Coarser sediments adjacent to the rim and peak would have experienced less compaction, and the central peak would have acted as a rigid indenter. This lateral gradient in the degree of compaction would have caused a rotation of younger strata toward the moat center, resulting in shallow dips away from the central peak for strata above the Murray formation (fig. S8). This mechanism may account for the regional dips observed from orbit (*55*) and provides an alternative to the interpretation that they were formed by mound-building accretion.

After maximum burial and crater infilling, wind-driven erosion resulted in partial exhumation of the crater-filling strata (Fig. 8D). Curiosity landed on nearly the lowest point of the exhumation surface, where fluvial-deltaic deposits were exposed, and then drove uphill to the south and across a facies transition into lacustrine sediments of the Murray formation. A final stage of fluvial activity occurred after exhumation, involving overland flow and sediment transport to create scattered fans (e.g., the Peace Vallis fan), possible deltas (*56*, *57*), and draping strata in the area explored by Curiosity (Fig. 1).

Crater statistics (*9*, *56*) indicate that the exhumation and exposure of most of the hundred to perhaps several hundred meters of strata exposed across Aeolis Palus and at the base of Mount Sharp had occurred by ~3.3 billion to 3.1 billion years ago (fig. S1). Hence, the available evidence suggests that the landscape acquired its present expression by the middle Hesperian Period, and this was followed by the long epoch of very slow eolian erosion that has continued to the present (*58*). These age constraints require infilling of the crater with sediments to (at least) the level of the top of the Murray formation; burial, compaction, and cementation of those sediments to form rocks; and subsequent erosion and exhumation of those rocks to form the lower reaches of the modern landscape, below the elevation of the hematite-bearing ridge—all within a few hundred million years of the crater's formation. The erosion rates are estimated to be ~200 m over ~400 million years, or 0.5 m per million years. If the crater was filled with even more sediment, as shown in Fig. 8, then these rates would be higher. In either case, these erosion rates must be adjusted for the time represented by crater infilling and therefore probably represent minimum estimates. We do not yet understand what drove exhumation on early Mars, but the rates indicated by our data are orders of magnitude faster than those calculated for more recent erosion of the martian surface [0.01 m per million years (*59*)]; they therefore more closely approximate long-term late Noachian to early Hesperian erosion rates for Mars (*60*) and long-term terrestrial erosion rates for Earth. Given that eroded materials must have been lifted out of the crater to form the existing moat, it seems that wind, rather than water, was the primary agent of erosion. Perhaps higher atmospheric pressure during this early phase of Mars's history (*61*) led to higher surface wind stresses and therefore higher rates of wind erosion (*62*).

The sediment source of the now-eroded sedimentary rocks was probably the Gale crater rim and walls, which are partly degraded and marked by incised drainage networks (supplementary text). On average, the floor of Gale crater is shallower than expected by 1.9 to 2.1 km, compared with other complex craters of similar diameter (*63*); this indicates crater infilling or crater rim lowering by this amount (figs. S9 and S10). The inferred amount of crater rim and wall erosion could have supplied more than enough sediment to account for both the Bradbury group and the Murray formation, as blankets of sediment that extended from the crater rim to the central peak (figs. S9 and S10). The current level of rim degradation can be accounted for by ~4.8 km of slope-parallel wall retreat (6.1% of the crater radius), which would generate a sediment layer ~600 m thick on average. Furthermore, an additional hundreds of meters of sediment could be created locally through erosion of the ~1000-km^2 Peace Vallis catchment, which is one of the few drainages to breach the Gale rim, and which sits directly upslope of the Bradbury group (figs. S9 and S10).

Paleoclimate

Noachian terrains are associated with broad mineralogical and morphological evidence for liquid water, including clay mineral–bearing bedrock, valley networks, open- and closed-basin lakes, and possibly a northern ocean. In contrast, Hesperian terrains provide evidence for water in the form of catastrophic outflows and hydrated sulfates, possibly indicating increased geothermal activity and volcanism. Gale crater formed at 3.8 billion to 3.6 billion years ago (*6*), toward the end of the Noachian Period, after the formation of the hemispheric dichotomy but perhaps coeval with the formation of the Tharsis bulge on the opposite side of the planet. Crater counts on various surfaces within Gale crater suggests that the crater-filling strata described here were deposited over a few hundred million years, extending into early Hesperian time (*6*, *9*, *56*).

Whereas the planetary-scale geomorphic influences on climate largely had arrived at their terminal states when Hesperian stream and lake systems at Gale crater were active, other influences were still evolving. Substantial enrichment in heavy isotopes is evident in multiple atmospheric species, including argon, carbon and oxygen in CO_2, and hydrogen and oxygen in water vapor (*64*–*66*). These results point to an initial atmospheric mass and water inventory in Mars's secondary atmosphere that were a few to many times greater than their present-day values. Mars's obliquity is poorly constrained during this time period, but it may have been large on average [mean value of 41.8° (*67*)]. Therefore, the latitudinal distribution of solar forcing, and thus climate and weather, are likely to have varied during this time period. Volcanism and impacts may have dramatically, if only temporarily, forced the climate during this era (*68*, *69*).

Yet even with an atmosphere substantially enhanced in CO_2, water, and other greenhouse gases derived from volcanic outgassing, models of Mars's climate (*70*–*72*) cannot reproduce global average temperatures that approach 273 K, which would make a straightforward case for abundant and geologically long-lived liquid water at the surface. In the absence of long-lived, globally warm temperatures, is regional or transient warming consistent with the geological record? Others have addressed this question for the martian valley networks and paleolakes, arguing that transient impact-induced warming or local meltwater from an icy Mars may have been capable of forming these features. For example, the Icy Highlands Scenario (*70*) posits that a cold but thicker atmosphere would glaciate the highland terrains but supply meltwater in volumes consistent with those needed to carve valleys and fill paleolakes.

In light of these cold climate scenarios, the absence of glaciogenic sedimentary deposits or fabrics in the Bradbury group and especially the Murray formation is notable. Coarse cobble or boulder conglomerates formed from tills have not been observed; frost wedges, indicative of strong oscillations in surface temperatures (*73*), are apparently absent. The well-exposed cross sections of strata exposed at Yellowknife Bay and in the valley systems at Dingo Gap, Kimberley, Hidden Valley, and Amargosa Valley do not reveal features that could be interpreted as frost wedges. Most importantly, well-laminated sediments of the Murray formation at Pahrump Hills form an ideal medium for frost wedges to be preserved, but none have been observed to date. Even if the Murray formation represents dry eolian sediments, formation of frost wedges would still be expected, as has been the case for extreme glacial events in dry environments on Earth (*73*). Finally, glacial dropstones were not observed in any of the subaqueous laminated facies. The climate recorded by the ~75 m of rock observed so far does not seem to have been frigid; the crater lake basin and its fringes, in ancient times, do not appear to have experienced glaciation or extreme cold. However, the increased influence of the adiabatic lapse rate in a thicker atmosphere may have created colder conditions on the crater rim. This is supported by geochemical data that indicate limited chemical weathering of sedimentary parent materials (*74*). Seasonal or glacial ice there could have supplied meltwater that transported sediment to the crater floor.

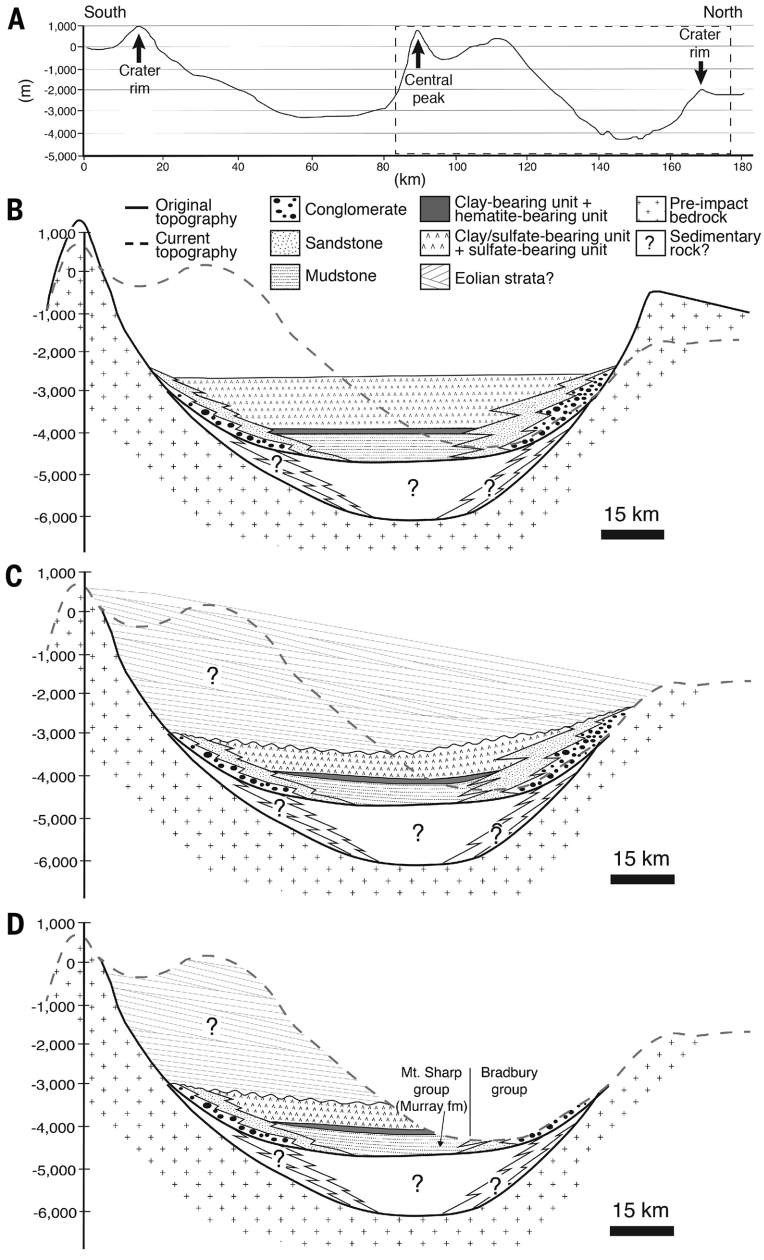

Fig. 8. History of the infilling of Gale crater and its exhumation to form Mount Sharp. (**A**) A north-south transect of the current topography, featuring the high southern rim, the crater's central peak at nearly equal elevation, the slightly lower false summit of Mount Sharp, and the much lower northern rim. The northern rim of Gale crater is assumed to have this lower elevation because it straddles the dichotomy boundary. The dotted box represents the part of the crater that is illustrated in (B), (C), and (D). (**B**) Early infilling of the crater during the aqueous period. The dashed line represents the modern topography, and the solid line represents the original post-impact topography, derived from the profiles of other craters of similar size and with central peaks of similar height The infilling of the crater was driven by erosion of the northern rim and the central peak, which generated sediment that was transported downslope, fining along the way due to hydraulic segregation of grain size. Crater diameter-depth relationships suggest that an additional 1 to 2 km of crater-infilling strata (pattern with question marks) may lie beneath the present-day surface (figs. S9 and S10). (**C**) During the subsequent dry period, the bulk of Mount Sharp formed via accumulation of eolian facies, very generally defined. The mass of Mount Sharp exerted a gravitational force that caused compaction of previously deposited strata, resulting in rotation of those strata downward relative to the rigid central peak (figs. S7 and S8). (**D**) Wind-driven erosion resulted in the exhumation of the crater-filling strata. Curiosity landed on nearly the lowest point of the exhumation surface, where fluvial-deltaic deposits were exposed, and then drove uphill to the south and across a facies transition into lacustrine sediments of the Murray formation.

This is supported by deuterium/hydrogen isotope ratios from ancient clays in a Gale lake deposit, which indicate that a global-equivalent layer of water of 100 to 150 m in thickness was present at the time of sediment accumulation (*75*).

Our in situ geological observations, which indicate a time series of deltaic-lacustrine complexes within Gale crater, raise additional questions for such cold climate models. The 1 to 4 m stratigraphic thickness of each delta deposit implies a body of standing water of at least that depth, which existed over a period of time long enough to accumulate that sediment and to allow delta foreset beds to prograde for at least many tens to possibly hundreds of meters. This implies that each lake was present for a time span on the order of 100 to 10,000 years, based on terrestrial analog rates (*16*, *76*, *77*).

These observations imply a minimum duration when each lake was stable both thermally (as liquid) and with respect to net evaporation and subsequent loss of water to colder regions. The latter effect can be overlooked if only volumetric constraints on water are considered (for example, tying the lake's formation to a transient climate event that supplies its initial volume via meltwater). Unless net evaporation is slowed by increased atmospheric humidity, or lakes are resupplied by runoff, a shallow lake can quickly evaporate. Open expanses of liquid water contained in numerous lakes or a hemispheric ocean would maintain atmospheric humidity and potentially allow for an active hydrological cycle.

The rover data allow for oscillations in the areal extent and depth of lakes between the major lake episodes associated with the deltas, including dry periods when eolian processes were dominant. Nevertheless, another key constraint implied by the observations is the total duration over which lake stability was possible, even if intermittent. Again using terrestrial analogs (*76*), we estimate that the stratigraphy traversed thus far by Curiosity (~75 m) would have required 10,000 to 10 million years to accumulate, and even longer if the ~150-m-thick Murray formation is included. Additionally, even though individual lakes may have come and gone, they were probably linked in time through a common groundwater table. Over the long term, this water table must have risen at least tens of meters to form the lakes that are marked by the deltas that Curiosity observed.

One of the key criteria for planetary habitability is the duration for which water might have been accessible to enable microbial origination and evolution. The Gale crater floor today is the lowest topographic depression for over a thousand kilometers in any direction, including the northern plains. Our results show that water pooled there, in surface and subsurface reservoirs, for a geologically and perhaps biologically relevant period of time.

REFERENCES AND NOTES

1. M. C. Malin, K. S. Edgett, Evidence for persistent flow and aqueous sedimentation on early Mars. *Science* **302**, 1931–1934 (2003). doi: 10.1126/science.1090544; pmid: 14615547
2. N. H. Warner, M. Sowe, S. Gupta, A. Dumke, K. Goddard, Fill and spill of giant lakes in the eastern Valles Marineris region of Mars. *Geology* **41**, 675–678 (2013). doi: 10.1130/G34172.1
3. T. J. Parker, J. A. Grant, B. J. Franklin, in *Lakes on Mars*, N. A. Cabrol, E. A. Grin, Eds. (Elsevier, Amsterdam, 2010), pp. 249–273.
4. R. M. Haberle *et al*., Eds., *The Atmosphere and Climate of Mars* (Cambridge Univ. Press, Cambridge, 2015).
5. J. P. Grotzinger *et al*., A habitable fluvio-lacustrine environment at Yellowknife Bay, Gale crater, Mars. *Science* **343**, 1242777 (2014). pmid: 24324272
6. B. J. Thomson *et al*., Constraints on the origin and evolution of the layered mound in Gale Crater, Mars using Mars Reconnaissance Orbiter data. *Icarus* **214**, 413–432 (2011). doi: 10.1016/j.icarus.2011.05.002
7. L. Le Deit *et al*., Sequence of infilling events in Gale Crater, Mars: Results from morphology, stratigraphy, and mineralogy. *J. Geophys. Res. Planets* **118**, 2439–2473 (2013). doi: 10.1002/2012JE004322
8. M. C. Malin, K. S. Edgett, Sedimentary rocks of early Mars. *Science* **290**, 1927–1937 (2000). doi: 10.1126/science.290.5498.1927; pmid: 11110654
9. M. C. Palucis *et al*., The origin and evolution of the Peace Vallis fan system that drains to the Curiosity landing area, Gale Crater, Mars. *J. Geophys. Res. Planets* **119**, 705–728 (2014). doi: 10.1002/2013JE004583
10. R. E. Milliken, J. P. Grotzinger, B. J. Thomson, Paleoclimate of Mars as captured by the stratigraphic record in Gale Crater. *Geophys. Res. Lett.* **37**, L04201 (2010). doi: 10.1029/2009GL041870
11. A. A. Fraeman *et al*., A hematite-bearing layer in Gale Crater, Mars: Mapping and implications for past aqueous conditions. *Geology* **41**, 1103–1106 (2013). doi: 10.1130/G34613.1
12. A. R. Vasavada *et al*., Overview of the Mars Science Laboratory mission: Bradbury Landing to Yellowknife Bay and beyond. *J. Geophys. Res. Planets* **119**, 1134–1161 (2014). doi: 10.1002/2014JE004622
13. R. M. E. Williams *et al*., Martian fluvial conglomerates at Gale crater. *Science* **340**, 1068–1072 (2013).pmid: 23723230
14. S. G. Fryberger, C. J. Schenk, Pin stripe lamination: A distinctive feature of modern and ancient eolian sediments. *Sediment. Geol.* **55**, 1–15 (1988). doi: 10.1016/0037-0738(88)90087-5
15. S. Patruno, G. J. Hampson, C. A. L. Jackson, Quantitative characterisation of deltaic and subaqueous clinoforms. *Earth Sci. Rev.* **142**, 79–119 (2015). doi: 10.1016/j.earscirev.2015.01.004
16. C. Pirmez, L. F. Pratson, M. S. Steckler, Clinoform development by advection-diffusion of suspended sediment: Modeling and comparison to natural systems. *J. Geophys. Res. Solid Earth* **103**, 24141–24157 (1998). doi: 10.1029/98JB01516
17. E. Mortimer, S. Gupta, P. Cowie, Clinoform nucleation and growth in coarse-grained deltas, Loreto basin, Baja California Sur, Mexico: A response to episodic accelerations in fault displacement. *Basin Res.* **17**, 337–359 (2005). doi: 10.1111/j.1365-2117.2005.00273.x
18. G. C. Nanson, Point bar and floodplain formation of the meandering Beatton River, northeastern British Columbia, Canada. *Sedimentology* **27**, 3–29 (1980). doi: 10.1111/j.1365-3091.1980.tb01155.x
19. J. Alexander, Nature and origin of a laterally extensive alluvial sandstone body in the Middle Jurassic Scalby Formation. *J. Geol. Soc. London* **149**, 431–441 (1992). doi: 10.1144/gsjgs.149.3.0431
20. A. Ielpi, M. Ghinassi, Planform architecture, stratigraphic signature and morphodynamics of an exhumed Jurassic meander plain (Scalby Formation, Yorkshire, UK). *Sedimentology* **61**, 1923–1960 (2014). doi: 10.1111/sed.12122
21. B. J. Willis, H. Tang, Three-dimensional connectivity of point-bar deposits. *J. Sediment. Res.* **80**, 440–454 (2010). doi: 10.2110/jsr.2010.046
22. G. H. Sambrook Smith, P. J. Ashworth, J. L. Best, J. Woodward, C. J. Simpson, The sedimentology and alluvial architecture of the sandy braided South Saskatchewan River, Canada. *Sedimentology* **53**, 413–434 (2006). doi: 10.1111/j.1365-3091.2005.00769.x
23. G. H. Sambrook Smith *et al*., The sedimentology and alluvial architecture of a large braid bar, Rio Parana, Argentina. *J. Sediment. Res.* **79**, 629–642 (2009). doi: 10.2110/jsr.2009.066
24. A. J. H. Reesink *et al*., Scales and causes of heterogeneity in bars in a large multi-channel river: Río Paraná, Argentina. *Sedimentology* **61**, 1055–1085 (2014). doi: 10.1111/sed.12092
25. C. M. Jones, Tabular cross-bedding in Upper Carboniferous fluvial channel sediments in the southern Pennines, England. *Sediment. Geol.* **24**, 85–104 (1979). doi: 10.1016/0037-0738(79)90030-7
26. R. S. Haszeldine, Fluvial bars reconstructed from a deep, straight channel, Upper Carboniferous coalfield of northeast England. *J. Sediment. Petrol.* **53**, 1233–1247 (1983).
27. D. M. Rubin, C. L. Carter, in *Bedforms and Cross-Bedding in Animation: SEPM Atlas Series No. 2* (Society for Sedimentary Geology, Tulsa, OK, 2006), Appendix 1.
28. E. D. McKee, Structures of dunes at White Sands National Monument, New Mexico (and a comparison with structures of dunes from other selected areas). *Sedimentology* **7**, 3–69 (1966). doi: 10.1111/j.1365-3091.1966.tb01579.x
29. C. Bristow, J. Pugh, T. I. M. Goodall, Internal structure of aeolian dunes in Abu Dhabi determined using ground-penetrating radar. *Sedimentology* **43**, 995–1003 (1996). doi: 10.1111/j.1365-3091.1996.tb01515.x
30. G. Kocurek *et al*., White Sands Dune Field, New Mexico: Age, dune dynamics and recent accumulations. *Sediment. Geol.* **197**, 313–331 (2007). doi: 10.1016/j.sedgeo.2006.10.006
31. J. P. Bhattacharya, in *Facies Models Revisited*, R. G. Walker, H. Posamentier, Eds. (Society for Sedimentary Geology, Tulsa, OK, vol. 84, 2006), pp. 237–292.
32. C. Olariu, J. P. Bhattacharya, Terminal distributary channels and delta front architecture of river-dominated delta systems. *J. Sediment. Res.* **76**, 212–233 (2006). doi: 10.2110/jsr.2006.026
33. S. Kostic, G. Parker, Progradational sand-mud deltas in lakes and reservoirs. Part 1. Theory and numerical modeling. *J. Hydraul. Res.* **41**, 127–140 (2003). doi: 10.1080/00221680309499956
34. D. A. Edmonds, R. L. Slingerland, Significant effect of sediment cohesion on delta morphology. *Nat. Geosci.* **3**, 105–109 (2010). doi: 10.1038/ngeo730
35. M. R. Gibling, N. S. Davies, Palaeozoic landscapes shaped by plant evolution. *Nat. Geosci.* **5**, 99–105 (2012). doi: 10.1038/ngeo1376
36. D. Winston, in *Fluvial Sedimentology*, A. D. Miall, Ed. (Canadian Society of Petroleum Geologists, Calgary, Canada, 1978), pp. 343–359.
37. D. G. F. Long, Architecture of pre-vegetation sandy-braided perennial and ephemeral river deposits in the Paleoproterozoic Athabasca Group, northern Saskatchewan, Canada as indicators of Precambrian fluvial style. *Sediment. Geol.* **190**, 71–95 (2006). doi: 10.1016/j.sedgeo.2006.05.006
38. R. H. Rainbird, Anatomy of a large-scale braid-plain quartzarenite from the Neoproterozoic Shaler Group, Victoria Island, Northwest Territories, Canada. *Can. J. Earth Sci.* **29**, 2537–2550 (1992). doi: 10.1139/e92-201
39. D. S. McCormick, J. P. Grotzinger, Distinction of marine from alluvial facies in the Paleoproterozoic (1.9 Ga) Burnside Formation, Kilohigok Basin, NWT, Canada. *J. Sediment. Petrol.* **63**, 398–419 (1993).
40. M. A. Martins-Neto, Braidplain sedimentation in a Proterozoic rift basin: The São João da Chapada Formation, southeastern Brazil. *Sediment. Geol.* **89**, 219–239 (1994). doi: 10.1016/0037-0738(94)90095-7
41. K. M. Bohacs, in *Lacustrine Sandstone Reservoirs and Hydrocarbon Systems*, O. W. Baganz, Y. Bartov, K. Bohacs, D. Nummedal, Eds. (AAPG Memoir 95, American Association of Petroleum Geologists, Tulsa, OK, 2012), pp. 13–56.
42. C. M. Bell, Quaternary lacustrine braid deltas on Lake General Carrera in southern Chile. *Andean Geol.* **36**, 51–65 (2009).
43. P. E. Potter, J. B. Maynard, P. J. Depetris, *Mud and Mudstones* (Springer, Berlin, 2005).
44. M. P. Lamb, J. P. Grotzinger, J. B. Southard, N. J. Tosca, in *Sedimentary Geology of Mars*, J. P. Grotzinger, R. E. Milken, Eds. (SEPM Special Publication No. 102, Society for Sedimentary Geology, Tulsa, OK, 2012), pp. 139–150.
45. C. C. Bates, Rational theory of delta formation. *Am. Assoc. Pet. Geol. Bull.* **37**, 2119–2162 (1953).
46. M. P. Lamb, B. McElroy, B. Kopriva, J. Shaw, D. Mohrig, Linking river-flood dynamics to hyperpycnal-plume deposits: Experiments, theory, and geological implications. *Geol. Soc. Am. Bull.* **122**, 1389–1400 (2010). doi: 10.1130/B30125.1
47. R. Y. Anderson, W. E. Dean, Lacustrine varve formation through time. *Palaeogeogr. Palaeoclimatol. Palaeoecol.* **62**, 215–235 (1988). doi: 10.1016/0031-0182(88)90055-7
48. B. Zolitschka, in *Encyclopedia of Quaternary Science*, S. A. Elias, Ed. (Elsevier, Amsterdam, 2007), pp. 3105–3114.
49. V. Ganti, K. M. Straub, E. Foufoula-Georgiou, C. Paola, Space-time dynamics of depositional systems: Experimental evidence

and theoretical modeling of heavy-tailed statistics. *J. Geophys. Res. Earth Surf.* **116**, F02011 (2011).
50. K. Pye, *Aeolian Dust and Dust Deposits* (Academic Press, London, 1987).
51. M. Pécsi, Loess is not just the accumulation of dust. *Quat. Int.* **7–8**, 1–21 (1990). doi: 10.1016/1040-6182(90)90034-2
52. R. E. Hunter, in *Recent and Ancient Nonmarine Depositional Environments: Models for Exploration*, F. G. Ethridge, R. M. Flores, Eds. (SEPM Special Publication No. 31, Society for Sedimentary Geology, Tulsa, OK, 1981), pp. 315–329.
53. D. M. Rubin, R. E. Hunter, Bedform climbing in theory and nature. *Sedimentology* **29**, 121–138 (1982). doi: 10.1111/j.1365-3091.1982.tb01714.x
54. R. B. Anderson, Geologic mapping and characterization of Gale Crater and implications for its potential as a Mars Science Laboratory landing site. *Mars* **5**, 76–128 (2010). doi: 10.1555/mars.2010.0004
55. E. S. Kite, K. W. Lewis, M. P. Lamb, C. E. Newman, M. I. Richardson, Growth and form of the mound in Gale Crater, Mars: Slope wind enhanced erosion and transport. *Geology* **41**, 543–546 (2013). doi: 10.1130/G33909.1
56. J. A. Grant, S. A. Wilson, N. Mangold, F. Calef III, J. P. Grotzinger, The timing of alluvial activity in Gale crater, Mars. *Geophys. Res. Lett.* **41**, 1142–1149 (2014). doi: 10.1002/2013GL058909
57. M. C. Palucis, thesis, University of California–Berkeley, Berkeley, CA (2014).
58. K. A. Farley *et al*., In situ radiometric and exposure age dating of the martian surface. *Science* **343**, 1247166 (2014). doi: 10.1126/science.1247166
59. M. P. Golombek *et al*., Erosion rates at the Mars Exploration Rover landing sites and long-term climate change on Mars. *J. Geophys. Res. Planets* **111**, E12S10 (2006).
60. N. H. Warner *et al*., Late Noachian to Hesperian climate change on Mars: Evidence of episodic warming from transient crater lakes near Ares Vallis. *J. Geophys. Res. Planets* **115**, E06013 (2010). doi: 10.1029/2009JE003522
61. H. Lammer *et al*., Outgassing history and escape of the martian atmosphere and water inventory. *Space Sci. Rev.* **174**, 113–154 (2013). doi: 10.1007/s11214-012-9943-8
62. J. C. Armstrong, C. B. Leovy, Long term wind erosion on Mars. *Icarus* **176**, 57–74 (2005). doi: 10.1016/j.icarus.2005.01.005
63. S. J. Robbins, B. M. Hynek, A new global database of Mars impact craters ≥1 km: 2. Global crater properties and regional variations of the simple-to-complex transition diameter. *J. Geophys. Res. Planets* **117**, E06001 (2012).
64. P. R. Mahaffy *et al*., Abundance and isotopic composition of gases in the martian atmosphere from the Curiosity rover. *Science* **341**, 263–266 (2013). pmid: 23869014
65. S. K. Atreya *et al*., Primordial argon isotope fractionation in the atmosphere of Mars measured by the SAM instrument on Curiosity and implications for atmospheric loss. *Geophys. Res. Lett.* **40**, 5605–5609 (2013). doi: 10.1002/2013GL057763; pmid: 25821261
66. C. R. Webster *et al*., Isotope ratios of H, C, and O in CO_2 and H_2O of the martian atmosphere. *Science* **341**, 260–263 (2013). doi: 10.1126/science.1237961; pmid: 23869013
67. J. Laskar *et al*., Long term evolution and chaotic diffusion of the insolation quantities of Mars. *Icarus* **170**, 343–364 (2004). doi: 10.1016/j.icarus.2004.04.005
68. T. L. Segura, O. B. Toon, A. Colaprete, Modeling the environmental effects of moderate-sized impacts on Mars. *J. Geophys. Res. Planets* **113**, E11007 (2008). doi: 10.1029/2008JE003147
69. I. Halevy, J. W. Head III, Episodic warming of early Mars by punctuated volcanism. *Nat. Geosci.* **7**, 865–868 (2014). doi: 10.1038/ngeo2293
70. R. Wordsworth *et al*., Global modelling of the early martian climate under a denser CO_2 atmosphere: Water cycle and ice evolution. *Icarus* **222**, 1–19 (2013). doi: 10.1016/j.icarus.2012.09.036
71. F. Forget *et al*., 3D modelling of the early martian climate under a denser CO_2 atmosphere: Temperatures and CO_2 ice clouds. *Icarus* **222**, 81–99 (2013). doi: 10.1016/j.icarus.2012.10.019
72. M. A. Mischna, V. Baker, R. Milliken, M. Richardson, C. Lee, Effects of obliquity and water vapor/trace gas greenhouses in the early martian climate. *J. Geophys. Res. Planets* **118**, 560–576 (2013). doi: 10.1002/jgre.20054
73. R. C. Ewing *et al*., New constraints on equatorial temperatures during a Late Neoproterozoic snowball Earth glaciation. *Earth Planet. Sci. Lett.* **406**, 110–122 (2014). doi: 10.1016/j.epsl.2014.09.017
74. S. M. McLennan *et al*., Elemental geochemistry of sedimentary rocks at Yellowknife Bay, Gale crater, Mars. *Science* **343**, 1244734 (2014). pmid: 24324274
75. P. R. Mahaffy *et al*., The imprint of atmospheric evolution in the D/H of Hesperian clay minerals on Mars. *Science* **347**, 412–414 (2015). doi: 10.1126/science.1260291; pmid: 25515119
76. P. M. Sadler, Sediment accumulation rates and the completeness of stratigraphic sections. *J. Geol.* **89**, 569–584 (1981). doi: 10.1086/628623
77. A. Cattaneo, F. Trincardi, L. Langone, A. Asioli, P. Puig, Clinoform generation on Mediterranean margins. *Oceanography* **17**, 104–117 (2004). doi: 10.5670/oceanog.2004.08

ACKNOWLEDGMENTS

The authors are indebted to the MSL project's engineering and management teams for their exceptionally skilled and diligent efforts in making the mission as effective as possible and enhancing science operations. We are also grateful to all those MSL team members who participated in tactical and strategic operations. Without the support of both the engineering and science teams, the data presented here could not have been collected. Helpful reviews were provided by K. Bohacs and two anonymous reviewers. Some of this research was carried out at the Jet Propulsion Laboratory, California Institute of Technology, under a contract with NASA. Work in the UK was funded by the UK Space Agency. Data presented in this paper are archived in the Planetary Data System (pds.nasa.gov).

SUPPLEMENTARY MATERIALS

www.sciencemag.org/content/350/6257/aac7575/suppl/DC1
Supplementary Text
Figs. S1 to S10
Tables S1 to S2
References (*78–103*)

8 June 2015; accepted 4 August 2015
10.1126/science.aac7575